Asymptotic electron motion in the strongly-radiation-dominated regime

A. S. Samsonov,[1,2] E. N. Nerush,[1,*] and I. Yu. Kostyukov[1,2]
[1]*Institute of Applied Physics, Russian Academy of Sciences, 46 Ulyanov Street, Nizhny Novgorod 603950, Russia*
[2]*Nizhny Novgorod State University, 23 Gagarin Avenue, Nizhny Novgorod 603950, Russia*

(Received 11 July 2018; published 29 November 2018)

We study electron motion in electromagnetic (EM) fields in the radiation-dominated regime. It is shown that the electron trajectories become close to some asymptotic trajectories in the strong-field limit. The description of the electron dynamics by these asymptotic trajectories significantly differs from the ponderomotive description that is barely applicable in the radiation-dominated regime. The particle velocity of the asymptotic trajectory is completely determined by the local and instant EM field. The general properties of the asymptotic trajectories are discussed. In most standing EM waves (including identical tightly focused counterpropagating beams) the asymptotic trajectories are periodic with the period of the wave field. Furthermore, for a certain model of the laser beam we show that the asymptotic trajectories are periodic in the reference frame moving along the beam with its group velocity, which may explain the effect of the radiation-reaction trapping.

DOI: 10.1103/PhysRevA.98.053858

I. INTRODUCTION

If the amplitude of an optical field is such that an electron gains in it energy of hundreds of its rest-mass energy, the electron starts to emit synchrotron radiation and can lose its energy efficiently [1]. This phenomenon, radiation reaction, is highly important for theoretical physics and astrophysics, therefore the motion of electrons in a strong laser field nowadays is a topic of numerous theoretical investigations [2–7] and it has been studied recently in experiments [8,9]. Also, the emission of hard photons by electrons in a strong laser field lets one make a femtosecond broadband source of MeV photons, based on a laser-pulse–electron-beam collision [10–12], laser-plasma interaction [13–17], or electromagnetic cascades [18,19]. In the interaction of a strong laser pulse with a plasma, radiation losses can significantly affect the plasma dynamics and, for instance, lead to less-efficient ion acceleration [20–24], the enhancement of the laser-driven plasma wakefield [25,26], highly efficient laser-pulse absorption [27], relativistic transparency reduction [28], and the inverse Faraday effect [29].

Despite the high importance of the radiation losses for laser-plasma physics at high intensity, there is no general concept of the losses' impact on the electron motion and this impact is considered mostly by *ad hoc* hypotheses and particle-in-cell (PIC) simulations. Only for a few field configurations are the analytical solutions for motion of emitting electron present [30–32], whereas for the motion of the nonemitting electron Miller's ponderomotive concept [33] is applicable in a vast number of cases.

In the high-intensity field, the energy gained by the electron can be significantly limited by the radiation losses. In this case, in contrast to the low-intensity limit, the electron Lorentz factor becomes small in comparison with the field amplitude: $\gamma/a_0 \ll 1$; here γ is the electron Lorentz factor and $a_0 = eE_0/mc\omega$ is the normalized amplitude of the electric field E_0, with ω the typical angular frequency of the field, c the speed of light, and m and $e > 0$ the electron mass and the magnitude of the electron charge, respectively. The smallness of γ/a_0 allows one to simplify the analytical treatment of the electron motion in the strongly-radiation-dominated regime. This can be illustrated by a stationary Zel'dowich solution [30] for the electron motion in the rotating electric field $\mathbf{E}(t)$. At moderate-field intensity the angle φ (between the particle velocity and the vector $-\mathbf{E}$) is connected with the electron Lorentz factor γ. However, in the strongly-radiation-dominated regime φ and γ/a_0 tend to zero (see Fig. 1) and the particle velocity coincides with the direction of the electric field ($\mathbf{v} \parallel \mathbf{E}$), thus γ is not needed in order to compute the particle trajectory.

In Refs. [34,35] the concept of the electron motion, which in the radiation-dominated regime can supersede the ponderomotive concept, is discussed. It was shown in Ref. [34] that in the regime of dominated radiation friction the number of degrees of freedom, which govern the electron motion, is reduced. Namely, it was shown for the rotating electric field with the Gaussian envelope that on timescales larger than the rotation period the electron position is described by a first-order differential equation that does not contain the electron momentum. For this, the electron motion with the Landau-Lifshitz radiation reaction has been considered. It was also shown that in the radiation-dominated regime, electrons are not expelled from but are captured for a long time by the strong-field region.

In Ref. [35] it is shown that for an almost arbitrary field configuration, in the strong-field limit in a timescale much smaller than the timescale of the field variation, the direction of the electron velocity approaches some certain direction that is determined only by the values of the local electric and magnetic fields. Then, as the electron velocity is known, the electron trajectory can be reconstructed. This approach, called

*nerush@appl.sci-nnov.ru

the low-energy limit, was used (but not described) for the fields of the linearly polarized standing waves [36].

Let us emphasize that if the electron velocity is determined not by the electron momentum but by the local fields, one can describe the plasma dynamics with hydrodynamical equations. Indeed, in this case the currents in Maxwell's equations depend only on the particle density and particle velocity [i.e., on the particle density and local electromagnetic (EM) fields], therefore the first-order equation for the electron position, together with Maxwell's equations and the continuity equation, forms a closed system of equations.

In this paper we present a step toward such a hydrodynamical approach to the plasma dynamics in the radiation-dominated regime. Namely, in Sec. II we estimate the γ/a_0 ratio and the threshold of the radiation-dominated regime. In Sec. III, for an arbitrary field configuration we find the first-order equation for the electron position, by a method different from that in Ref. [35] and with the B case (discussed below) considered separately. The right-hand side of this equation is the velocity field that is fully determined by the local-field vectors. It is shown that $\gamma \ll a_0$ is enough for this first-order equation to be valid in the laser field. In Sec. IV we compare the solution of this first-order equation with the solution of the exact equations of the electron motion for a number of field configurations. In Sec. V we discuss the relation between the velocity field and the Poynting vector. In Sec. VI the symmetry of the velocity field induced by the symmetry of the Maxwell equations is considered and the dramatic difference between the ponderomotive description and the description by the velocity field in the radiation-dominated regime is demonstrated. Thus, in Sec. VI A, in the limit of strong fields, the electron motion in a wide class of periodic standing waves is shown to be periodic. From this, in Sec. VI B we show with a certain model of the laser beam that the beam can capture the electrons and carry them along itself with the beam group velocity. Section VII is a summary.

II. STRONGLY-RADIATION-DOMINATED REGIME

In order to estimate the threshold value of the normalized field amplitude a_0 for the radiation-dominated regime, let us start from the equations of the electron motion with the Landau-Lifshitz radiation reaction force incorporated,

$$\frac{d\mathbf{p}}{dt} = -\mathbf{E} - \mathbf{v}\times\mathbf{B} - F_{rr}\mathbf{v}, \tag{1}$$

$$\frac{d\gamma}{dt} = -\mathbf{v}\mathbf{E} - F_{rr}v^2, \tag{2}$$

where time is normalized to $1/\omega$, $\mathbf{v}$ is the electron velocity normalized to the speed of light c, $\mathbf{p} = \gamma\mathbf{v}$ is the electron momentum normalized to mc, $\mathbf{E}$ and $\mathbf{B}$ are the electric and magnetic fields, respectively (normalized to $mc\omega/e$), and $F_{rr}\mathbf{v}$ is the main term of the radiation reaction force [37]

$$F_{rr} = \alpha\gamma^2\frac{2}{3}\frac{\hbar\omega}{mc^2}\{(\mathbf{E}+\mathbf{v}\times\mathbf{B})^2 - (\mathbf{E}\mathbf{v})^2\}. \tag{3}$$

Here $\alpha = e^2/\hbar c \approx 1/137$ is the fine-structure constant and ω is the frequency characterizing the timescale or the space scale of the field (e.g., angular frequency of the laser field).

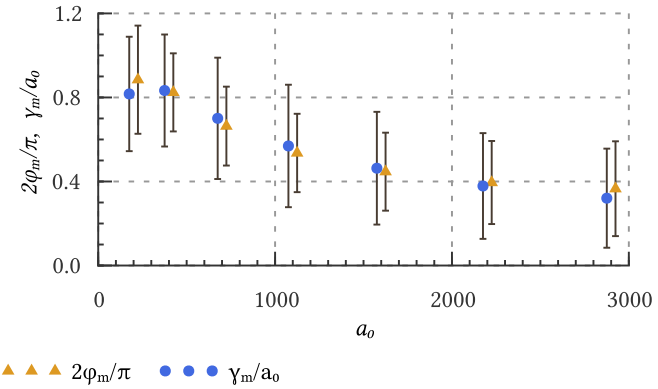

FIG. 1. Electrons moving in the rotating electric field and experiencing a quantum radiation reaction for many periods of the rotation. Circles show the ratio of the mean Lorentz factor γ_m to a_0 and triangles the mean angle φ_m between the particle velocity and the vector opposite to the electric field, for different values of the field amplitude a_0. Bars depict the standard deviations $\pm\sigma$. Results of the PIC MC simulations are for the field angular frequency $\omega = 2\pi c/\lambda$, with $\lambda = 1\ \mu$m.

The radiation losses increase sharply with the increase of γ, therefore for some electron Lorentz factor $\gamma = \bar{\gamma}$, the further energy gain stops due to the losses. The corresponding value $\bar{\gamma}$ can be found from Eq. (2) assuming that the transverse and the longitudinal to $\mathbf{v}$ components of the Lorentz force are of the order of a_0,

$$\bar{\gamma} \approx \sqrt{\frac{3}{2\alpha a_0}\frac{mc^2}{\hbar\omega}}, \tag{4}$$

where a_0 is the characteristic electric-field strength. In the absence of the radiation reaction the electron energy in the field can be estimated as $\gamma \sim a_0$, thus the radiation-dominated regime corresponds to $\bar{\gamma} \ll a_0$, hence

$$a_0 \gg a_0^* = \left(\frac{3}{2\alpha}\frac{mc^2}{\hbar\omega}\right)^{1/3}. \tag{5}$$

Note that, for the laser wavelength $\lambda = 1\ \mu$m, the amplitude $a_0^* \approx 440$ corresponds to the intensity $I \approx 5\times10^{23}\ \mathrm{W\,cm^{-2}}$. This level of intensity is expected to be reached in the near future with facilities such as ELI-beamlines [38], ELI-NP [39], Apollon [40], Vulcan 2020 [41], or XCELS [42].

In the case of strong radiation losses the angle between the Lorentz force and the electron velocity can be small and the transverse to $\mathbf{v}$ component of the Lorentz force becomes much lower than the longitudinal one. However, this does not affect much the given estimates. For instance, for the electron motion in the rotating electric field from the stationary Zel'dowich solution [30] we get $\varphi \approx \gamma/a_0$ and $\gamma \approx (a_0/\mu)^{1/4} \ll a_0$ (where $\mu = 2\alpha\hbar\omega/3mc^2$) at $a_0 \gg a_0^*$, with the same estimate for a_0^* (except the factor $3/2$ in the parentheses; see Ref. [30]). Note also that the quantum consideration of the radiation reaction gives results that are close to the Zel'dovich solution: In the Monte Carlo (MC) simulations the mean φ value is about $\pi/2$ times larger than γ/a_0 and γ/a_0 drops with the increase of the field amplitude (Fig. 1). In what follows we assume that the field is far beyond the threshold of the radiation-dominated regime, $a_0 \gg a_0^*$.

III. VELOCITY FIELD AND ASYMPTOTIC TRAJECTORIES

The reduced equations of the electron motion for arbitrary field configuration can be derived as follows. The equation for the electron velocity can be obtained from Eqs. (2) and (1) as

$$\frac{d\mathbf{v}}{dt} = -\frac{1}{\gamma}\left\{\mathbf{E} - \mathbf{v}(\mathbf{vE}) + \mathbf{v}\times\mathbf{B} + \frac{F_{rr}\mathbf{v}}{\gamma^2}\right\}, \tag{6}$$

where the first three terms in curly brackets approximately correspond to the transverse to $\mathbf{v}$ component of the Lorentz force. If the angle ψ between the Lorentz force and the electron velocity is noticeable ($\psi \sim 1$), then the term with F_{rr} in Eq. (6) is negligible, because $F_{rr}/\gamma^2 \sim a_0^2\alpha\hbar\omega/mc^2 \ll a_0$ for reasonable field amplitudes $E_0 \lesssim E_S/\alpha$, where $E_S = m^2c^3/e\hbar$ is the Sauter-Schwinger critical field. Thus, as long as $\gamma \ll a_0$, we have $|d\mathbf{v}/dt| \gg 1$. This means that the characteristic timescale of the velocity vector variation is small, $\tau_\mathbf{v} \sim \gamma/a_0 \ll 1$. Therefore, on small timescales it can be assumed that the fields $\mathbf{E}$ and $\mathbf{B}$ in Eq. (6) are constant. In the constant EM field the electron velocity $\mathbf{v}$ in a time of some $\tau_\mathbf{v}$ approaches some asymptotic direction. This direction corresponds to $\psi \to 0$, hence $d\mathbf{v}/dt = 0$, and can be found as follows.

A. The *B* case

In the case of $\mathbf{E}\cdot\mathbf{B} = 0$ and $B > E$ there is a reference frame K' in which the field is purely magnetic and $\mathbf{B}' \parallel \mathbf{B}$ (here a prime denotes a quantity in K'). In K' the electron goes along the helical path with its axis parallel to the direction of $\mathbf{B}'$. The corresponding drift velocity of the electron in the laboratory reference frame K is the speed of K' in K and can be found from

$$\mathbf{E} + \mathbf{v}\times\mathbf{B} = 0. \tag{7}$$

We note that Eq. (7) does not depend on the component of the velocity parallel to the magnetic field, so one can choose this component arbitrarily (implying $v < 1$). One can choose, for example, the solution with $\mathbf{v}\cdot\mathbf{B} = 0$, i.e.,

$$\mathbf{v} = \frac{\mathbf{E}\times\mathbf{B}}{B^2}. \tag{8}$$

As shown in Sec. VI B, the ambiguity of $\mathbf{v}$ in this case can be resolved by additional physical considerations.

B. The *E* case

If $\mathbf{E}\cdot\mathbf{B} \neq 0$ or $E > B$ there is a reference frame K' in which $\mathbf{E}' \parallel \mathbf{B}'$ or $B' = 0$. The electron trajectory in K' asymptotically approaches the straight line parallel to $\mathbf{E}'$ and v approaches 1. Note that for the resulting electron trajectory $\mathbf{v}\cdot\mathbf{E} < 0$ as long as the electron is accelerating by the field.

As $v \approx 1$ and the electron moves along the straight line, in the laboratory reference frame K the resulting $\mathbf{v}$ can be found from the equation $d\mathbf{v}/dt = 0$, which yields

$$\mathbf{E} - \mathbf{v}(\mathbf{vE}) + \mathbf{v}\times\mathbf{B} = 0. \tag{9}$$

Scalar multiplication of Eq. (9) by $\mathbf{B}$, $\mathbf{E}$, and $\mathbf{E}\times\mathbf{B}$ leads to the solution

$$\mathbf{vB} = \frac{\mathbf{EB}}{\mathbf{vE}}, \tag{10}$$

$$\mathbf{v}\cdot\mathbf{E}\times\mathbf{B} = E^2 - (\mathbf{vE})^2, \tag{11}$$

$$\mathbf{vE} = -\sqrt{\frac{E^2 - B^2 + \sqrt{(E^2-B^2)^2 + 4(\mathbf{EB})^2}}{2}}, \tag{12}$$

$$\mathbf{v}\cdot\mathbf{E}\times[\mathbf{E}\times\mathbf{B}] = (\mathbf{vE})(\mathbf{EB}) - (\mathbf{vB})E^2. \tag{13}$$

The right-hand side of Eq. (12) is relativistic invariant and we choose the sign $-$ in order to obtain the stable trajectory in K'. For the opposite sign $+$, the electron in K' is decelerating and its velocity is reversed quickly if initially $\mathbf{v}$ is not exactly parallel to the direction given by Eq. (9). Note that vectors $\mathbf{E}$, $\mathbf{E}\times\mathbf{B}$, and $\mathbf{E}\times[\mathbf{E}\times\mathbf{B}]$ form an orthogonal basis, thus Eqs. (11)–(13) are enough to determine $\mathbf{v}$ unambiguously.

C. Asymptotic trajectory

Considering the electron motion on a timescale of the field variation timescale $t \sim 1 \gg \tau_\mathbf{v}$, one can neglect the dynamics of the electron while it is approaching the constant-field-approximation asymptotic solution and assume that in every time instant the electron velocity is determined by Eq. (7) or (9), which depend only on the instant (and local) fields. Thus, the electron trajectory is governed by the reduced-order equations

$$\frac{d\mathbf{r}}{dt} = \mathbf{v}, \tag{14}$$

$$\mathbf{E} - \mathbf{v}(\mathbf{vE}) + \mathbf{v}\times\mathbf{B} = 0. \tag{15}$$

Equation (15) determines the velocity field $\mathbf{v}$ and can be used in both B and E cases [in the B case it yields Eq. (7)]. From here on we call the solution of Eqs. (14) and (15) an asymptotic trajectory because, first, locally it corresponds to the asymptotic ($t \to \infty$) electron trajectory in the constant-field approximation, and second, it describes the electron trajectory in the asymptotically strong field ($a_0 \gg a_0^*$).

Note that the reasoning about the electron trajectory in the radiation-dominated regime is also valid if the parameter χ is large [$\chi \approx \gamma F_\perp/eE_s$ (see Refs. [43,44]), where $F_\perp$ is the component of the Lorentz force perpendicular to the particle velocity]. In this case ($\chi \gg 1$) the synchrotron emission is described by the quantum formulas and Eq. (3) is not valid, however, it is still possible to describe the electron trajectory classically between the photon emission events [43,45] because $\ell_f \ll \ell_W$. Here $\ell_f \sim mc^2/F_\perp$ is the radiation formation length, i.e., the distance within which the emission of a single photon occurs, and $\ell_W \sim c/W$ is the mean distance that the electron passes without the photon emission; W is the full probability rate of the photon emission. Estimating

$$W \sim \frac{mce^2}{\hbar^2}\frac{\chi^{2/3}}{\gamma}, \tag{16}$$

we obtain $\ell_f/\ell_W \sim \alpha/\chi^{1/3} < 1/137 \ll 1$. Therefore, the electron moves classically between the short events of the

photon emission. Note also that for optical frequencies $\ell_W/\lambda \sim \hbar\omega/\alpha\chi^{2/3}mc^2 \ll 1$.

IV. SIMPLE EXAMPLES

In order to test the asymptotic description of the electron trajectory [Eqs. (14) and (15)] we compare numerical solutions of them with numerical solutions of the classical equations of the electron motion with the radiation reaction taken into account by the inclusion of the Landau-Lifshitz force [37] or by the recoil of the emitted photons described in the quasiclassical framework of Baier *et al.* [43,45]. Numerical solution of the full equations of the electron motion is based on Vay's pusher [46], where the Landau-Lifshitz force is taken into account with Euler's method or, alternatively, the quantum recoil is taken into account by the MC technique similarly to the QUILL [47,48] code (see also Appendix A). In order to solve Eqs. (14) and (15) we use the classical Runge-Kutta method. The test results for various field configurations are present below.

A. Rotating electric field

In the rotating electric field of the amplitude a_0 Eq. (15) gives $\mathbf{v} = -\mathbf{E}/E$, which coincides with the high-field limit ($a_0 \gg a_0^*$) of Zel'dovich's stationary solution [30] utilizing the main term of the Landau-Lifshitz force. This stationary solution can be updated by taking into account quantum corrections to the radiation-reaction force [49], which also yields $\mathbf{v} \to -\mathbf{E}/E$ in the high-field limit. Monte Carlo simulations demonstrate the same behavior, however, high dispersion of the angle between $\mathbf{v}$ and $\mathbf{E}$ is evident (see Fig. 1).

B. Static *B* node

Let us start from the simple field configuration

$$E_y = a_0, \quad B_z = a_0 x, \tag{17}$$

and the other components of the fields are zero. In Fig. 2 the velocity field (8) ($|x| > 1$) and Eqs. (11) and (12) ($|x| \leqslant 1$) are depicted by the arrows. In the left half of Fig. 2 the electron trajectories computed with the Landau-Lifshitz force are shown, and in the right half of Fig. 2 the electron trajectories are computed with the Monte Carlo technique and quantum synchrotron formulas. Obviously, the shape of the electron trajectories computed with the Monte Carlo approach is slightly different for different runs, so the bars depict the standard deviation of the electron's final position. The trajectories are computed for different a_0 values, namely, $a_0 = 500$, 2×10^3, and 1×10^4, which correspond to the dashed, dash-dotted, and solid lines, respectively. First, it can be seen that at higher-a_0 values the real electron velocity coincides better with the velocity field that induces the asymptotic trajectories. Second, the Landau-Lifshitz approach demonstrates slightly better coincidence, because in the Landau-Lifshitz approach the mean electron energy is generally less than in the quantum approach. Note that the fields (17) resemble the *B* node of a standing linearly polarized wave, however, in the linearly polarized standing wave the sign of $\mathbf{E}\times\mathbf{B}|_x$ varies in time and the node attracts the asymptotic electron trajectories during one half of a period and repels them during the other half.

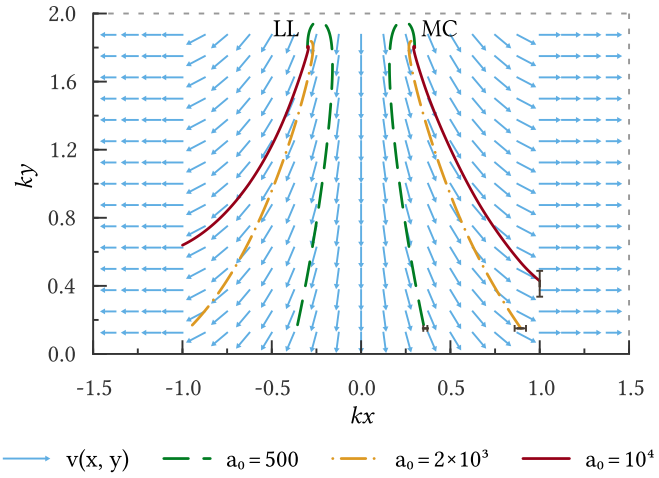

FIG. 2. Velocity field (15) (arrows) and the full electron trajectories in the fields (17) for different values of the field magnitude: $a_0 = 500$ (dashed lines), $a_0 = 2\times10^3$ (dash-dotted lines), and $a_0 = 1\times10^4$ (solid lines). The electrons start from $x_0 = \pm0.3$ with the Lorentz factor $\gamma_0 = 100$ and the momentum along the y axis. The trajectories at $x < 0$ are computed with the Landau-Lifshitz radiation reaction taken into account, while the trajectories at $x > 0$ are computed with the radiation reaction taken into account by Monte Carlo technique and quantum formulas (A12). Bars depict the standard deviation $\pm\sigma$ of the final electron position computed with 400 trajectories. The coordinates are normalized to $1/k = \lambda/2\pi$, where $\lambda = 1$ μm.

C. Linearly polarized standing wave

In the linearly polarized standing wave asymptotic electron trajectories can be found analytically. The fields of the linearly polarized standing wave read

$$\mathbf{E} = \mathbf{y}_0 a_0 \cos(t)\cos(x), \tag{18}$$

$$\mathbf{B} = \mathbf{z}_0 a_0 \sin(t)\sin(x), \tag{19}$$

where $\mathbf{y}_0$ and $\mathbf{z}_0$ are the unit vectors along the y and z axes, respectively. Then from Eqs. (8), (11), and (12) we get

$$\mathbf{v} = \begin{cases} \mathbf{x}_0 \tan(t)\tan(x) \pm \mathbf{y}_0\sqrt{1-\tan^2(t)\tan^2(x)}, & E > B \\ \mathbf{x}_0 \cot(t)\cot(x), & E < B. \end{cases} \tag{20}$$

Since the fields are homogeneous along the y axis the electron's motion along it is not of any interest. Then $x(t)$ of the asymptotic trajectory is found from the algebraic equations

$$\sin(x)\cos(t) = \sin(x_0)\cos(t_0), \quad E > B \tag{21a}$$

$$\cos(x)\sin(t) = \cos(x_0)\sin(t_0), \quad E < B, \tag{21b}$$

where the starting point $x_0 = x(t_0)$ also belongs to the region $E > B$ or $E < B$. For instance, the electron trajectory initially is determined by Eq. (21a), then it reaches the point with $E = B$, and after that the trajectory is determined by Eq. (21b) up to the moment when the electron reaches another point with $E = B$, and so on. For $E = B$ Eqs. (18) and (19) yield

$$|\tan(x)\tan(t)| = 1, \tag{22}$$

with the solution

$$x = \pm t + \frac{\pi}{2} + \pi n, \quad n = 0, \pm 1, \pm 2, \ldots. \tag{23}$$

For the electron starting from the point x_0 at the moment $t_0 = 0$ the chain of points $(x_1, t_1), (x_2, t_2), \ldots$ at which $E = B$ is the following. First, from Eqs. (21) and (22) under the assumption that initially $E > B$, we have

$$\cot x_1 = \tan t_1 = \sqrt{\frac{1}{\cos(x_0)} - 1}. \tag{24}$$

The coordinate x_2 can be found from the observation that $x_2 = x_1$ and $t_2 = \pi - t_1$ obey Eq. (21b) with x_0 and t_0 replaced by x_1 and t_1. Also, $x_2 = x_1$ and $t_2 = \pi - t_1$ obey Eq. (22) (because x_1 and t_1 obey them). Analogously, $x_3 = x_2$ and $t_3 = \pi + t_1$. Then the electron trajectory periodically repeats itself [see Fig. 3(a)].

Note that the electron trajectory in the linearly polarized standing wave is periodic in the framework of the presented asymptotic theory. As shown in Sec. VI A, this is just an example of the general behavior of the electron trajectories in standing waves in the radiation-dominated regime. However, it can seem that this behavior contradicts the anomalous radiative trapping (ART) [36]. Really, ART is caused by a drift of the electron between the asymptotic trajectories given by Eqs. (21). This drift takes many periods of the field [36] and cannot be described by the presented asymptotic theory.

The asymptotic electron trajectories computed with Eqs. (14) and (15) are shown in Fig. 3(a) with thin pale dotted and solid lines [the computed trajectories coincide exactly with the analytical solutions (21)]. Six electron trajectories computed with Vay's pusher and Monte Carlo technique for the photon emission are also depicted: for $a_0 = 1\times10^3$ by green lines (starting at $x < 0$) and for $a_0 = 1\times10^4$ by red lines (starting at $x < 0$). Figure 3(b) shows the energy of the electrons on trajectories A and B from Fig. 3(a). The coincidence of the electron trajectories computed for $a_0 = 1\times10^4$ with the asymptotic trajectories is evident, opposite to the $a_0 = 1\times10^3$ case in that the condition $\gamma \ll a_0$ is not fulfilled. Note that in the case of $a_0 = 1\times10^4$ the electrons moving according to the MC approach for the radiation reaction become closer to the B nodes for each subsequent period, which is the effect of ART.

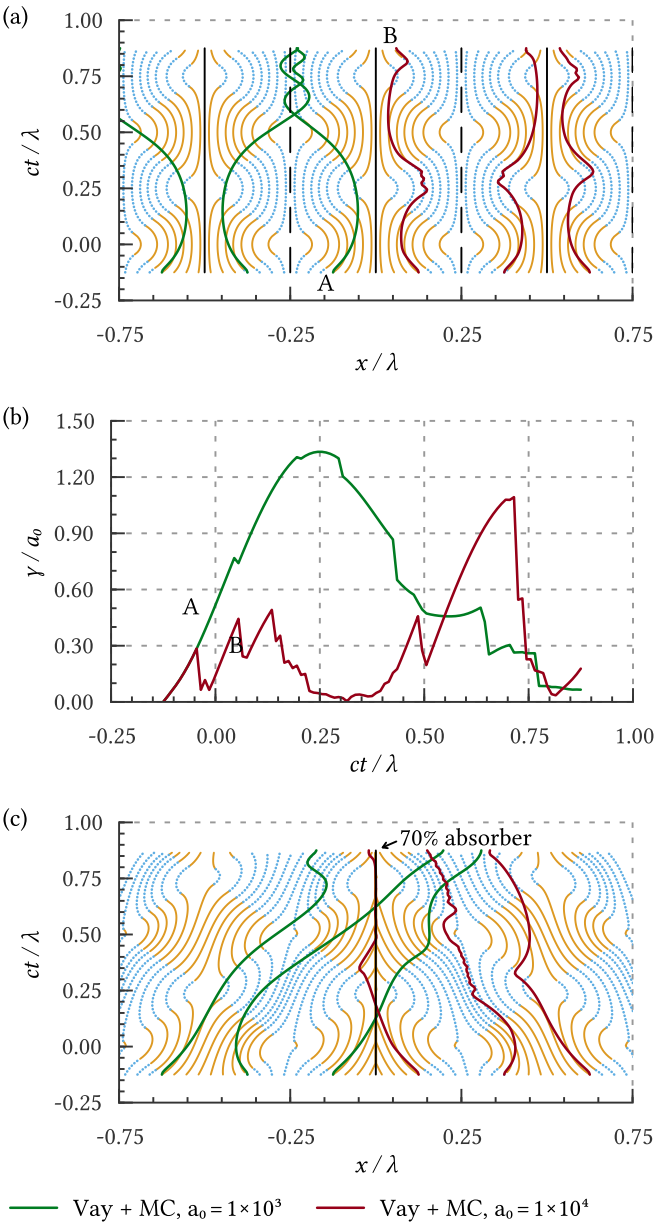

FIG. 3. Electron motion (a) and (b) in the field of the linearly polarized standing electromagnetic wave (18) and (19) and (c) in the field of two counterpropagating linearly polarized waves with a plane at $x = 0$ absorbing 70% of the incoming energy [see Eqs. (25) and (26), $R = 0.55$]. Pale lines depict asymptotic trajectories obtained by the numerical integration of Eq. (14) for the E and B cases (solid thin beige line and dotted blue line, respectively). Dark thick lines correspond to the numerical integration of the classical electron motion equations with the quantum radiation reaction (A12) taken into account by Monte Carlo technique, for $a_0 = 1\times10^3$ and $a_0 = 1\times10^4$ (starting at $x < 0$ and $x > 0$, respectively). It is worth mentioning that the pale lines in (a) coincide with the analytical solution (21) and with the thin green lines in Fig. 2 from Ref. [36].

V. ABSORPTION-INDUCED TRAPPING

It follows from Eqs. (8) and (11) that the angle between the asymptotic velocity $\mathbf{v}$ and the Poynting vector $\mathbf{S} \propto \mathbf{E} \times \mathbf{B}$ is always less than $\pi/2$, i.e., $\mathbf{v} \cdot \mathbf{S} > 0$. This hints that the electron motion in the radiation-dominated regime can be connected with the energy flow of the electromagnetic fields. Let us consider the region containing currents which (partially) absorb the incoming electromagnetic wave. On average, the Poynting vector is directed into the region of the currents, and we suggest that in the radiation-dominated regime this region attracts the electron trajectories. In this section we verify this suggestion in a couple of examples.

A plane wave pushes initially immobile electrons approximately in the direction of the Poynting vector, so it can seem that the absorption-induced trapping can be realized without a strong radiation reaction. However, as seen from the examples below, in the absence of strong radiation losses, if the electrons have been accelerated by a wave, then they cannot be turned back by a counterpropagating wave. Thus the

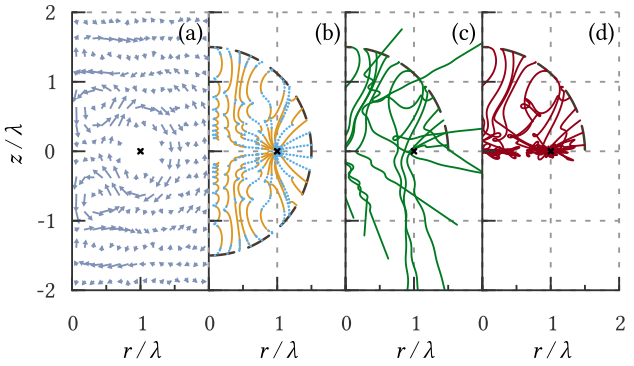

FIG. 4. (a) Magnetic field of a multipole wave that is entirely absorbed by a current loop (see Appendix B); the loop radius is $r_\ell = \lambda = 1\ \mu$m and $t = 0$. The axis of the loop coincides with the z axis and the position of a wire is shown by the black cross. (b) Asymptotic electron trajectories for the E and B cases (solid beige and dotted blue lines, respectively) in the multipole wave. The electrons start to move at $t = 0$ from the points on the circle $(r^2 + z^2)^{1/2} = 1.5r_\ell$ (thick black dashed line). The Vay-MC electron trajectories in the field of the multipole wave are for (c) $I_0 = 1\times10^3$ and (d) $I_0 = 5\times10^3$. All trajectories are computed for $t \in [0, 5\lambda/c]$.

radiation reaction may cause electron trapping in the region with strong absorption of the electromagnetic energy.

A. Counterpropagating linearly polarized waves partially absorbed by a plane

The field of two counterpropagating linearly polarized (along the y axis) waves, which is partially absorbing at the plane $x = 0$, can be written as

$$\mathbf{E} = \mathbf{y}_0 a_0\{\cos(t)\cos(x) - 0.5(1 - R)\cos(x \mp t)\}, \quad (25)$$

$$\mathbf{B} = \mathbf{z}_0 a_0\{\sin(t)\sin(x) \mp 0.5(1 - R)\cos(x \mp t)\}, \quad (26)$$

where in $\mp$ the upper sign corresponds to $x > 0$ and the lower one corresponds to $x < 0$, and R is the reflection coefficient. The asymptotic and Vay-MC electron trajectories in this field are shown in Fig. 3(c) with the same color codes as in Fig. 3(a). Here $R = 0.55$, which means absorption of 70% of the wave energy in the plane $x = 0$. As can be seen from the figure, the electron trajectories are attracted by the plane $x = 0$ in the strongly-radiation-dominated regime, whereas at moderate intensity of the waves the electrons easily pass the plane. The mean standard deviation of x computed for the Vay-MC electron trajectories for ten periods of the wave and $x_0 = 0.25\lambda$ is about 1.5λ for $a_0 = 1\times10^3$ and 0.2λ for $a_0 = 1\times10^4$.

B. Multipole wave absorption by a current loop

The field of a multipole harmonic wave that is completely absorbed by a current loop can be obtained by time reversal of the field emitting by a current loop (see Appendix B). The electron motion in the absorbing multipole wave with the angular frequency $\omega = 2\pi c/\lambda$ for a loop radius $r_\ell = \lambda = 1\ \mu$m is shown in Fig. 4, where in the cylindrical coordinate system the wire position is marked with the black cross. The z axis is the axis of the loop. Figure 4(a) demonstrates the magnetic field of the multipole wave at $t = 0$. Figure 4(b) shows the asymptotic electron trajectories and Figs. 4(c) and 4(d) show the electron trajectories computed by the Vay-MC algorithm for the loop current magnitude $I_0 = 1\times10^3$ and for $I_0 = 5\times10^3$, respectively. The trajectories start at $t = 0$ from the sphere shown by a thick dashed line and are computed up to $t = 5\lambda/c$.

In the region very close to the wire the field gradient is huge, hence the scale of the field change can be less than the radiation formation length. Thus, strictly speaking, more accurate consideration of the radiation reaction near the wire should be used. However, as discussed in Sec. III C, it does not generally matter that an exact form of the radiation reaction is used, because for the asymptotic description to be valid it is enough that the electron Lorentz factor is small in comparison with the field amplitude.

It can be seen from Fig. 4 that the current loop attracts the asymptotic electron trajectories. However, it can be seen that the absorption-induced trapping is not really a strict trapping but just means that electrons in the radiation-dominated regime stay for a long time in the region with the currents absorbing the incoming waves.

VI. EMISSION-ABSORPTION SYMMETRY AND GENERAL PROPERTIES OF ASYMPTOTIC TRAJECTORIES

In this section we consider the properties of the electron trajectories described by Eqs. (14) and (15). For this purpose let us consider the well-known symmetry of the Maxwell equations, namely, the transforms

$$t^* = -t, \quad (27)$$

$$\mathbf{E}^* = -\mathbf{E}, \quad (28)$$

$$\mathbf{B}^* = \mathbf{B}, \quad (29)$$

$$\rho^* = -\rho, \quad \mathbf{j}^* = \mathbf{j} \quad (30)$$

do not change them, i.e., they lead to the Maxwell's equations for the starred variables; here ρ is the charge density and $\mathbf{j}$ is the current density. From here on we refer to $\mathbf{E}$, $\mathbf{B}$, and $\mathbf{j}$ evolving in time t as the initial system and $\mathbf{E}^*$, $\mathbf{B}^*$, and $\mathbf{j}^*$ evolving in time t^* as the starred system. This symmetry is the relation between a system of currents emitting some fields and the system of currents absorbing the fields, namely, the Poynting vector, the $\mathbf{j}\cdot\mathbf{E}$ product, and the time direction in the starred system is opposite to that in the initial system.

According to Eq. (15), in the starred system the velocity field $\mathbf{v}^*$ relates to the velocity field of the initial system $\mathbf{v}$ as

$$\mathbf{v}^*(\mathbf{r}, t^*) = -\mathbf{v}(\mathbf{r}, -\mathbf{t}^*), \quad (31)$$

which obeys the stability condition $\mathbf{v}^*\cdot\mathbf{E}^* < 0$. Thus, in the starred system the velocity field and the time direction are opposite to that in the initial system, which leads to the same trajectories in the starred system $\mathbf{r}^*(t^*)$ as in the initial system, passed by the electrons in the opposite direction: $d\mathbf{r}^*/dt^* = \mathbf{v}^*(\mathbf{r}^*, t^*) = -\mathbf{v}(\mathbf{r}^*, -t^*)$.

We note a fundamental difference between the asymptotic trajectories described by Eqs. (15) and (14) and by the ponderomotive description. The ponderomotive force is determined by the distribution of E^2 and B^2 and is indifferent to the transforms (27)–(30), whereas these transforms reverse direction of the electron motion in the case when Eqs. (15) and (14) are applicable, namely, when radiation reaction is strong.

In order to illustrate the difference between the ponderomotive description and the description by the velocity field (15) the following toy example can be considered. An electron is scattered by two compact counterpropagating laser pulses initially separated by some distance. The first one propagates, say, along the direction $\mathbf{x}_0$ and the second pulse is formed from the first one with the substitution (27)–(29), thus it propagates in the direction $-\mathbf{x}_0$. We suppose that the electron initially is closer to the first laser pulse that hence scatters the electron aside (if we consider the task in the framework of the ponderomotive description). In this case the electron can move far away from the pulses and the field of the second laser pulse is then unimportant. However, if the radiation reaction is strong, the asymptotic approach should be valid. In this case the trajectory of the electron in the field of the second laser pulse is the same as in the field of the first one but the electron passes the trajectory in the opposite direction [see Eq. (31)]. Therefore, in the radiation-dominated regime, the electron after its motion in the field of the first laser pulse will be brought back to its initial position by the second laser pulse that differs strongly from that the ponderomotive approach predicts.

Thus, the asymptotic description of the electron motion (14) and (15) implies that the electrons are not scattered by, but stay for a long time in the field of a laser pulse or in a laser beam. This conclusion is in good agreement with the results of theoretical considerations and numerical simulations showing that the ponderomotive force can be significantly suppressed by the radiation reaction [34,50].

A. Asymptotic trajectories in standing waves

We see in Sec. IV that the reduced equations lead to periodic electron trajectories in the linearly polarized standing electromagnetic wave. Here we show that Eqs. (14) and (15) always lead to periodic electron trajectories in a wide class of fields, namely, in the periodic fields which can be represented in the form

$$\mathbf{E} = \mathbf{f}(\mathbf{r}, t) - \mathbf{f}(\mathbf{r}, -t), \tag{32}$$

$$\mathbf{B} = \mathbf{g}(\mathbf{r}, t) + \mathbf{g}(\mathbf{r}, -t), \tag{33}$$

where $\mathbf{E} = \mathbf{f}(\mathbf{r}, t)$ and $\mathbf{B} = \mathbf{g}(\mathbf{r}, t)$ are the solution of Maxwell's equations for some charge density ρ and current density $\mathbf{j}$ (for the sake of simplicity let us consider $\rho = 0$ and $\mathbf{j} = 0$). This representation means that the fields are the sum of the fields of some system and the fields of the corresponding starred system. In this case the symmetry (27)–(30) leads to the same fields of the starred system as in the initial system, i.e., $\mathbf{E}^*(\mathbf{r}, t^*) = \mathbf{E}(\mathbf{r}, t^*)$ and $\mathbf{B}^*(\mathbf{r}, t^*) = \mathbf{B}(\mathbf{r}, t^*)$, hence it should lead to the same velocity field $\mathbf{v}^*(\mathbf{r}, t^*) = \mathbf{v}(\mathbf{r}, t^*)$, which together with Eq. (31) yields

$$\mathbf{v}(\mathbf{r}, -t) = -\mathbf{v}(\mathbf{r}, \mathbf{t}). \tag{34}$$

Thus, the velocity field in the electromagnetic fields (32) and (33) is an odd function of time. Consequently, the time reversal conserves the equation for the electron position

$$\frac{d\mathbf{r}}{d(-t)} = \mathbf{v}(\mathbf{r}, (-t)) \tag{35}$$

and the electron position $\mathbf{r}(t)$ is an even function of time. Therefore,

$$\begin{aligned}\mathbf{r}(t) - \mathbf{r}(-t) &= \int_{-t}^{t} \mathbf{v}(\mathbf{r}(t), t)dt \\ &= \int_0^t \mathbf{v}(\mathbf{r}(t), t)dt + \int_0^t \mathbf{v}(\mathbf{r}(-t), -t)dt = 0.\end{aligned} \tag{36}$$

As long as the velocity field governed by Eqs. (8) and (10)–(13) is a single-valued function of the electromagnetic fields and the fields are periodic in time, the velocity field is also periodic with the same period, T. Thus, the velocity field is an odd function relative to any time instant $t = nT$, where n is an integer. The electron starts to move at $t = nT - T/2$, then it comes to the starting point a period later $\mathbf{r}(nT + T/2) = \mathbf{r}(nT - T/2)$, and then due to the periodicity of $\mathbf{v}$ at $t = (n + 1)T$, we have $\mathbf{r}[(n + 1)T + T/2] = \mathbf{r}(nT + T/2)$. Therefore, in the framework of the asymptotic approach, the electron is moving periodically back and forth along the same path in the periodic fields Eqs. (32) and (33).

B. Asymptotic trajectories in a laser beam of finite diameter

Here we stress that many field configurations could be reduced to the form of periodic fields that obey the emission-absorption symmetry (27)–(30). In the preceding section we also assumed that the velocity field is a single-valued function of the fields. This is not strictly true in the B case, because one can add to $\mathbf{v}$ from Eq. (8) a vector parallel to $\mathbf{B}$. The effect of this ambiguity is also discussed in this section.

Let us consider the fields of the TE11 mode of a rectangular metallic waveguide

$$E_x = 0, \tag{37}$$

$$E_y = a_0 \cos(k_y y) \sin(k_z z) \cos(t - k_x x), \tag{38}$$

$$E_z = -\frac{a_0 k_y}{k_z} \sin(k_y y) \cos(k_z z) \cos(t - k_x x), \tag{39}$$

$$B_x = \frac{a_0 \left(k_z^2 + k_y^2\right)}{k_z} \cos(k_y y) \cos(k_z z) \sin(t - k_x x), \tag{40}$$

$$B_y = -k_x E_z, \tag{41}$$

$$B_z = k_x E_y, \tag{42}$$

where we assume that the wave angular frequency $\Omega = (k_x^2 + k_y^2 + k_z^2)^{1/2} = 1$ (here we use the normalization frequency ω equal to the frequency of the wave and, as before, the time is normalized to $1/\omega$, coordinates are normalized to c/ω, and $\mathbf{k}$

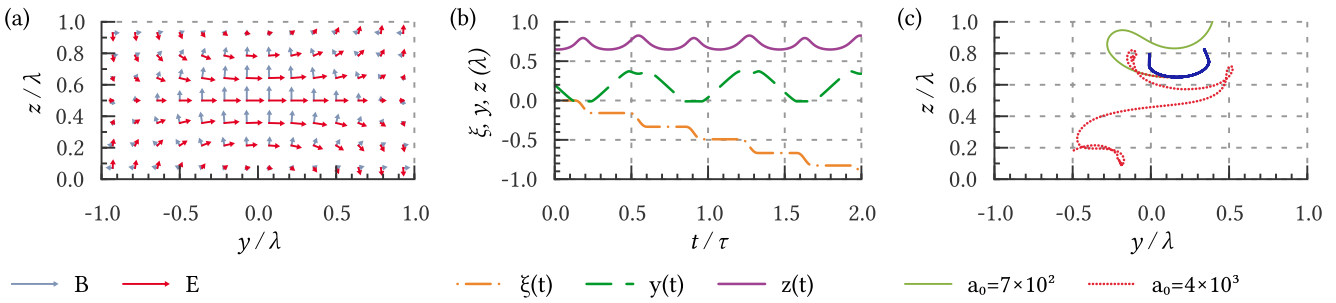

FIG. 5. (a) Electric and magnetic fields (red and blue arrows, respectively; the electric field is mostly horizontal) of the continued TE11 mode of a waveguide [Eqs. (38) and (39) and Eqs. (41) and (42), respectively] at $t = 0$. (b) Asymptotic trajectory of an electron computed with Eqs. (14), (8), and (10)–(13) in the laboratory reference frame; $\xi = x - v_g t$, where v_g is the group velocity of the TE11 mode. (c) Same asymptotic trajectory (dark thick line) and typical electron trajectories starting at the point $x = 0$, $y = 0.2\,\lambda$, and $z = 0.65\,\lambda$ ($\lambda = 1\ \mu$m and $t \in [0, 2\tau]$), for $a_0 = 700$ (solid thin green line) and $a_0 = 4\times10^3$ (dotted red line).

is the wave number normalized to ω/c). These fields obey the metallic boundary conditions at $y = 0, \pm\ell_y, \pm2\ell_y, \ldots$ ($E_z = 0$) and at $z = 0, \pm\ell_z, \pm2\ell_z, \ldots$ ($E_y = 0$). Here $\ell_y = \pi/k_y$ and $\ell_z = \pi/k_z$ are the sizes of the waveguide along the y and z axes, respectively.

The fields (37)–(42) are the solution of the Maxwell equations not only inside the waveguide but in the open space as well because these fields can be represented as a sum of plane waves. In particular, we consider these fields in the region $y \in [-\ell_y/2, \ell_y/2]$ and $z \in [0, \ell_z]$ as the model of the laser beam of finite diameter. If $\ell_y \gg \ell_z$, the electric field is mainly directed along the y axis and reaches its maximum in the center of the beam.

The fields (37)–(42) are shown in Fig. 5(a) for $\ell_y = 4\pi$, $\ell_z = 2\pi$, and $t = x = 0$. The asymptotic electron trajectory computed for these fields is shown in Fig. 5(b), where $\xi = x - v_g t$, $v_g = k_x \approx 0.83$ is the group velocity of the electromagnetic wave, and the trajectory starts at $t = 0$, $x = 0$, $y = 0.2$, and $z = 0.65$ and is computed up to $t = 2\tau$, where

$$\tau = \frac{2\pi}{k_x(v_\phi - v_g)} = \frac{2\pi}{1 - k_x^2} \tag{43}$$

is the intrinsic timescale of the task and $v_\phi = 1/v_g$ is the phase velocity of the wave. For Fig. 5 $c\tau/\lambda \approx 3.2$. In Figs. 5(c) and 5(d) the same asymptotic trajectory is shown as the thick blue line. Five electron trajectories in the fields given by Eqs. (37)–(42) are shown in Figs. 5(c) and 5(d). These trajectories start at the same point as the asymptotic trajectory, but they are computed by Vay's algorithm with a quantum radiation reaction incorporated by the Monte Carlo technique. For Figs. 5(c) and 5(d) we use $a_0 = 700$ and $a_0 = 4\times10^3$, respectively.

It can be seen from Figs. 5(b)–5(d) that the asymptotic trajectory is quasiperiodic, which is in qualitative agreement with the fact that for $a_0 = 4\times10^3$ the electrons stay for a long time in the high-field region. However, as we will see below, the asymptotic trajectories being computed in the laboratory reference frame yield the values of ξ and the values of the trajectory period which do not coincide well with that for real electron trajectories. The reason for that is that Eq. (8) is not Lorentz invariant, namely, if one computes $\mathbf{v}$ from it in some reference frame, in another reference frame one obtains $\mathbf{v}' = E' \times B' + aB'$, where a is a constant.

Let us transform the fields (37)–(42) to the reference frame K' moving along the x axis with the group velocity of the fields v_g. This lead to the fields

$$E_y' = a_0 k_\perp \cos(k_y y)\sin(k_z z)\cos(k_\perp t'), \tag{44}$$

$$E_z' = -\frac{a_0 k_\perp k_y}{k_z}\sin(k_y y)\cos(k_z z)\cos(k_\perp t'), \tag{45}$$

$$B_x' = \frac{a_0\left(k_z^2 + k_y^2\right)}{k_z}\cos(k_y y)\cos(k_z z)\sin(k_\perp t'), \tag{46}$$

$$E_x' = B_x' = B_y' = B_z' = 0, \tag{47}$$

where $k_\perp = \sqrt{1 - k_x^2}$. These fields do not depend on x' and for all the electrons in these fields the component of the Lorentz force along the x' axis is absent. Furthermore, the electrons due to the radiation reaction "forget" their initial direction of motion, hence we conclude that the average velocity of the electrons in the fields (44)–(47) is $v_x' = 0$. Therefore, in K the average electron velocity is $v_x = v_g$, hence $\xi = \text{const}$, which is in good agreement with the results of Vay-MC simulations. Note that $\xi = \text{const}$ does not coincide with the result of the asymptotic consideration in the laboratory reference frame [see Fig. 5(b)]. Also, a wrong value of v_x leads to a wrong value of the period of y and z coordinates of the electron in the framework of the asymptotic approach.

The substitution $t' \to t' + \pi/2k_\perp$ yields that the electric field given by Eqs. (44) and (45) are odd functions of time and the magnetic field (46) is an even function of time in K'. As follows from Sec. VI A, in this case the electron trajectories are periodic in the radiation-dominated regime and their period is equal to $2\pi/k_\perp$ in K'. Therefore, in the laboratory reference frame in the radiation-dominated regime the electrons move along the x axis with the group velocity of the laser beam and, as $y' = y$ and $z' = z$, the electron trajectories are periodic in the yz plane with the period

$$\frac{2\pi}{k_\perp\sqrt{1 - v_g^2}} = \tau. \tag{48}$$

Thus, the ambiguity of the velocity field in the asymptotic approach can be resolved by an appropriate choose of the reference frame.

Therefore, we show that the asymptotic description (14) and (15) leads to periodic trajectories in a wide class of standing waves (e.g., formed by laser beams of finite diameter) and to electron motion along the laser beam with its group velocity with periodic transverse motion. The latter may explain the effect of the radiation-reaction trapping [50].

VII. CONCLUSION

We have shown that in the radiation-dominated regime electrons tend to move with velocity that is determined by the fields only [see Eq. (15)]. This means that the electron trajectory can be found from the first-order equation (14). We call this velocity asymptotic because it can be found as the asymptotic electron velocity ($t \to \infty$) in the constant-field approximation. The reason for reduction of the equation order is that the electron energy in the radiation-dominated regime is small ($\gamma \ll a_0$) and the electrons are "light" and are easily turned by the laser field to the asymptotic direction in a time much shorter than the characteristic variation time of the electromagnetic fields. The velocity field $\mathbf{v}(\mathbf{r}, t)$ corresponds to the absence of the component of the Lorentz force transverse to the electron velocity, so $\mathbf{v}$ is also called the radiation-free direction [35].

In a number of the electromagnetic-field configurations we found the numerical solutions of the reduced-order equations and the full equations of electron motion with the radiation reaction taken into account by the Monte Carlo technique and the Baier *et al.* synchrotron formulas [43]. The comparison between these solutions demonstrated that the reduced-order equations can be used for a qualitative description of the electron trajectories for a_0 greater than or of the order of 1000 for optical wavelengths. In order to stress these high values of a_0 we referred to the solutions of the reduced equations of motion as asymptotic trajectories ($a_0 \to \infty$).

Also we demonstrated that the reduced-order equations for the electron trajectories in the radiation-dominated regime are a useful analytical tool. First, they predict the electron trapping in the regions where the wave field is absorbed (see Sec. V). This result can be important for the theoretical consideration of the field absorption by the QED cascade in the counterpropagating laser waves [18]. Second, contrary to the concept of the ponderomotive force, the asymptotic theory leads to periodic electron trajectories in a wide class of standing electromagnetic fields (including the case of counterpropagating tightly focused laser beams; see Sec. VI A). This result is in good agreement with Ref. [34], which demonstrates the reduction of the ponderomotive force in the radiation-dominated regime. Furthermore, using a certain configuration of the laser beam, we demonstrated that the beam in the radiation-dominated regime does not push the electrons aside, but captures and carries them with the group velocity of the beam. This result probably explains the radiation-reaction trapping observed in the numerical simulation of Ref. [50].

Therefore, the concept of the ponderomotive force is not applicable in the radiation-dominated regime and can be replaced by the description of the asymptotic electron trajectories. The latter implies that velocities of the electrons at a given point are the same and hence the electrons (positrons) in the radiation-dominated regime can be described in the framework of the hydrodynamical approach. Maxwell's equations, in which the electron current is determined only by the plasma density and by the local field values [see Eq. (15)], together with the continuity equation for the plasma density, form the closed system of equations. Note that the reduced-order equations give the positive field work on the electrons ($\mathbf{v} \cdot \mathbf{E} < 0$), hence the plasma in the framework of the asymptotic theory is always an absorbing medium. This hydrodynamical approach has been tested in Ref. [51], where PIC simulations demonstrate that the spread of the electron velocity direction can be high even at high intensities, however, on average the direction of the electron velocity coincides with the asymptotic velocity. This allows one to obtain a dispersion relation for an extremely intense circularly polarized wave in an electron-positron plasma.

ACKNOWLEDGMENTS

We thank A. V. Bashinov and V. A. Kostin for fruitful discussions. We are grateful to E. V. Frenkel, who brought to our attention the symmetries of Maxwell's equations, and to T. Docker for his help with the HASKELL-CHART library. This research was supported by the Grants Council under the President of the Russian Federation (Grant No. MK-2218.2017.2). The study of the absorption-induced trapping was supported by the Russian Science Foundation through Grant No. 18-11-00210.

APPENDIX A: TESTS OF NUMERICAL INSTRUMENTS

1. Radiation reaction: Classical limit

In order to test Vay's solver for the equations of motion [46] coupled with the Landau-Lifshitz radiation reaction force (taken into account by Euler method) let us consider electron motion in constant crossed electric and magnetic fields

$$E_y = a_0/2, \quad B_z = a_0, \tag{A1}$$

$$E_x = E_z = B_x = B_y = 0. \tag{A2}$$

In the reference frame K' moving along the x axis with the speed $V = 0.5$ the electric field vanishes and only the z component of the magnetic field remains, $B'_z = B_z\sqrt{1 - V^2}$, where the prime denotes quantities in K'. Taking into account the Landau-Lifshitz radiation reaction, for relativistic electron motion in K' we obtain (assuming $\gamma \gg 1$)

$$d\gamma'/dt' = -C\gamma'^2, \tag{A3}$$

$$dw'/dt' = iB'_z w'/\gamma', \tag{A4}$$

$$dv'_z/dt' = 0, \tag{A5}$$

where

$$C = \frac{2}{3}\frac{e^2}{\hbar c}\frac{\hbar\omega}{mc^2}B'^2_z v^2_\perp, \tag{A6}$$

$w' = v'_x + iv'_y$, $v_\perp^2 = v_x'^2 + v_y'^2$, and ω is just some frequency used for normalization of time. The solutions of Eqs. (A3)–(A5) are

$$\gamma' = \frac{\gamma'_0}{1+\gamma'_0 C t'}, \tag{A7}$$

$$w' = w'_0 \exp\left[\frac{iB'_z}{\gamma'_0}\left(t' + \frac{\gamma_0 C t'^2}{2}\right)\right], \tag{A8}$$

and

$$x' + iy' = x'_0 + iy'_0 + w'_0\sqrt{\frac{i\pi}{2B'_z C}}\exp\left(-\frac{iB'_z}{2\gamma_0'^2 C}\right) \times\left\{\operatorname{erf}\left[\sqrt{\frac{B'_z C}{2i}}\left(t' + \frac{1}{\gamma'_0 C}\right)\right] - \operatorname{erf}\left(\sqrt{\frac{B'_z C}{2i}}\frac{1}{\gamma'_0 C}\right)\right\}, \tag{A9}$$

where the subscript 0 denotes $t' = 0$ and

$$\operatorname{erf}(x) = \frac{2}{\sqrt{\pi}}\int_0^x \exp(-t^2)\,dt \tag{A10}$$

is the error function.

Figure 6(a) demonstrates the electron trajectory in the xy plane obtained with the numerical integration of the equation of motion, taking into account the radiation reaction in Landau-Lifshitz form (solid blue line) for $a_0 = 50.3$, $\omega = 2\pi c/\lambda$, $\lambda = 1.1$ nm, $x_0 = y_0 = 0$, $v_x(t=0) \simeq 0.8$, $v_z(t=0) \simeq 0.6$, and $\gamma_0 = 63$. Note that these parameters ensure $v'_\perp(t) = v'_x(t=0) = 0.5 = V$, leading in the laboratory reference frame to the cycloidlike trajectory with points of $dy/dx \to \infty$.

For the given parameters we obtain $B'_z = 43.6$, $\gamma'_0 = \gamma'(t'=0) = 43.6$, and $C = 4.9\times10^{-3}$, and from Eq. (A7) at the time instant $t'_1 = 6\pi$ we get $\gamma'(t'_1) = \gamma'_0/5$. Neglecting displacement of the particle x' and assuming $v'_x(t'_1) = V$, we finally get for the laboratory reference frame $t_1 = (1-V^2)^{-1/2}t'_1 \approx 22$ and $\gamma(t_1) \approx 12.6$. It should be mentioned that at the time instance at which $v'_x = V$, in the laboratory reference frame the Lorentz factor reaches its local maximum. A numerical solver using the Landau-Lifshitz force demonstrates that the local maximum of γ closest to $t_1 = 22$ is reached at $t \approx 21.5$ and is $\gamma \approx 13.4$, which is quite close to the predicted value.

Equation (A9) yields $y'(t' \to \infty) \approx 0.463$ for the above-mentioned parameters. This value $[y(t\to\infty) = y'(t'\to\infty)]$ is depicted as a dotted gray line in Fig. 6 and is in good agreement with the value obtained with the numerical solver. The dashed orange line is obtained by means of a particle pusher, which takes into account the quantum formulas and is described in the next section.

2. Radiation reaction: General case

The quantum radiation reaction can be taken into account in Vay's pusher by means of the Monte Carlo technique. To do this we use the alternative event generator [44] based on the Baier *et al.* synchrotron formula [37,45]. The event generator checks at every time step if the photon emission occurs, and if it does, the electron momentum is decreased on the momentum of the emitted photon. Using the classical description of the electron trajectory together with the quantum formula for the photon emission is valid because the radiation formation length in strong fields ($a_0 \gg 1$) is much smaller than the field characteristic scale [37,45,52].

In order to test Vay's pusher coupled with a Monte Carlo event generator we compute the energy distribution of the electrons in the crossed fields (A1) and (A2). The resulting spectra are compared with the spectra obtained from the Boltzmann equation in the reference frame K'.

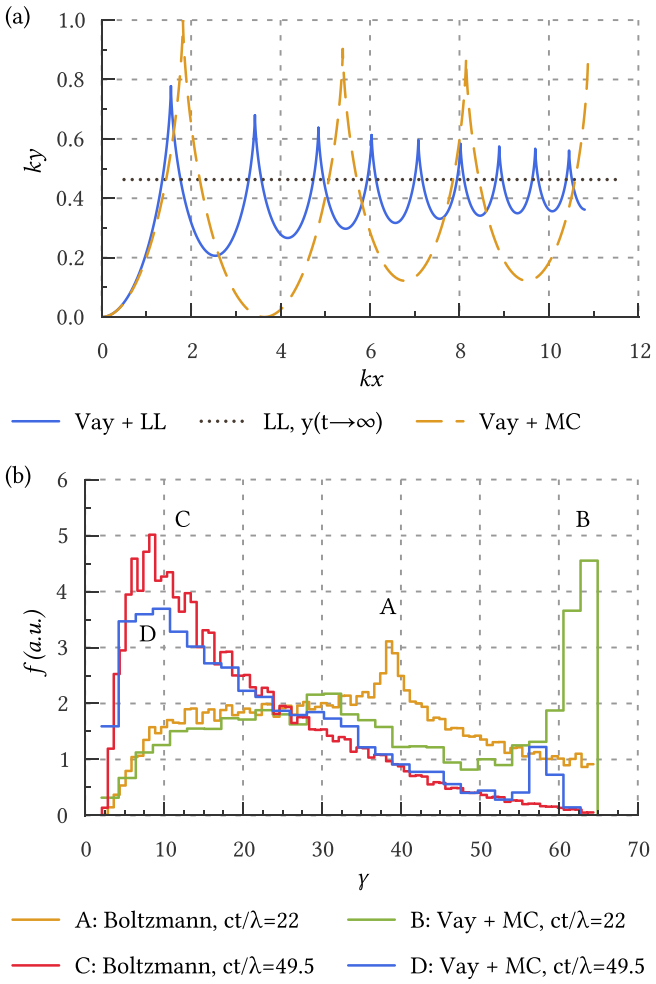

FIG. 6. (a) Electron trajectory in the crossed electric and magnetic fields (A1) and (A2) ($a_0 = 50.3$ and $\lambda = 1.1$ nm) computed by numerical integration of the classical equations of the electron motion with the radiation reaction taken into account by means of the main term of the Landau-Lifshitz radiation reaction force (solid line) and by means of Monte Carlo technique and quantum emission probability (A12) (dashed line). The dotted line depicts $y(t\to\infty)$ found from Eq. (A9). The electrons initially have $v_x \simeq 0.8$, $v_z \simeq 0.6$, and $\gamma = 63$. (b) In the same fields, the energy distribution of the electrons with the same initial momentum, computed by the same method as for the dashed line in (a) (lines B and D) and with numerical integration of the Boltzmann equation (A11), for different time instants. The coordinates are normalized to $1/k = \lambda/2\pi$, where $\lambda = 1.1\times10^{-3}$ μm.

As mentioned above, in the reference frame K' moving along the x axis with velocity $V = 0.5$ the electrons experience the pure magnetic field directed along the z axis. Therefore, in K' the Boltzmann equation that describes the electron energy distribution $f'(t', \gamma')$ is

$$\frac{\partial f'(t', \gamma')}{\partial t'} = \int_{\gamma'}^{\infty} w(\epsilon, \epsilon - \gamma') f'(t', \epsilon) d\epsilon - W(\gamma') f'(t', \gamma'), \tag{A11}$$

where

$$w(\epsilon, \epsilon_\gamma) = -\frac{\alpha}{\epsilon_\ell \epsilon^2}\left[\int_{\varkappa}^{\infty} \mathrm{Ai}(\xi) d\xi + \left(\frac{2}{\varkappa} + \frac{\epsilon_\gamma \chi \varkappa^{1/2}}{\epsilon}\right) \mathrm{Ai}'(\varkappa)\right] \tag{A12}$$

is the distribution of the photon emission probability by the electron with the Lorentz factor ϵ over the photon energy ε_γ normalized to mc^2, i.e., over $\epsilon_\gamma = \varepsilon_\gamma / mc^2$ (see Refs. [37,45]), and

$$\chi = \epsilon_\ell B'_z v_\perp \epsilon, \tag{A13}$$

$$\varkappa = \left[\frac{\epsilon_\gamma}{(\epsilon - \epsilon_\gamma)\chi}\right]^{2/3}, \tag{A14}$$

$$W(\gamma') = \int_0^{\gamma'} w(\gamma', \epsilon_\gamma) d\epsilon_\gamma \tag{A15}$$

is the overall emission probability for an electron with the Lorentz factor γ', and $\epsilon_\ell = \hbar\omega / mc^2$, with ω the frequency used for normalization of time.

The Boltzmann equation (A11) can be solved numerically as follows. In the finite-difference method the distribution function $f'(\gamma')$ is represented as a vector and the right-hand side of Eq. (A11) is represented as the product of a matrix and a vector. Then the Euler method can be used and the computation of $f'(t', \gamma')$ from $f'(t' = 0, \gamma')$ is reduced to a matrix exponentiation, which can be done with a square-and-multiply algorithm that has logarithmic complexity of the number of time steps. Then the distribution function in the initial reference frame can be found from $f'(t', \gamma')$ with Lorentz transformation. For that one should neglect the electron displacement in K' [i.e., $x'(t') - x'(0)$] and assume that in K' the angles φ' between the x' axis and $\mathbf{v}'_\perp$ are uniformly distributed on the interval $[0, 2\pi)$,

$$t = t'\Gamma, \tag{A16}$$

$$\gamma = \gamma'\Gamma(1 + V v_\perp \cos\varphi'), \tag{A17}$$

$$f(\gamma) \propto \int f'(\gamma') \frac{d\gamma'}{d\gamma} d\varphi' = \int \frac{f'(\gamma')}{1 + V v_\perp \cos\varphi'} d\varphi', \tag{A18}$$

where the integration should be performed over the path determined by the value of γ and Eq. (A17), and $\Gamma = (1 - V^2)^{-1/2}$. It is worth noting that for correctness of the method the step along γ' in the finite-difference scheme should be much smaller than the width of the emission spectrum. Thus, especially a small step of γ' should by used in the classical regime.

Figure 6(b) demonstrates the electron spectra in the crossed fields (A1) and (A2) with $a_0 = 50.3$ and $\lambda = 1.1$ nm used for the normalization. The electrons initially (at $t = 0$) move along the x and z axes ($v_x \simeq 0.8$ and $v_z \simeq 0.6$) and have the Lorentz factor $\gamma_0 = 63$. Curves A and C are obtained by Eq. (A11) for $t = 22$ and $t = 49.5$, respectively. Curves B and D represent the spectra of 8000 particles whose trajectory is computed by Vay's pusher coupled with a Monte Carlo event generator, for $t = 22$ and $t = 49.5$, respectively.

In K' the parameters of the simulations yield the quantum parameter $\chi'(t' = 0) = 2$, and if a Landau-Lifshitz radiation reaction is used, χ' drops down to $\chi'(t = 22) = 0.4$ and $\chi'(t = 49.5) = 0.1$ [see Eq. (A7)]. However, initially $\chi' \gtrsim 1$, which leads to a wide emission spectrum and a wide resulting spectrum of the electrons. Moreover, the overall emission probability is not very high and a significant fraction of electrons do not emit photons at all. These electron fractions form peaks clearly seen on curves A and B. The position of the peak on curve A corresponds to nonemitting electrons with $v'_x = -0.5$, which according to Eq. (A17) gives $\gamma \approx 38$. However, in the Monte Carlo simulation at $t = 22$ the distribution of electrons over φ' is far from the uniform one and most of the nonemitting electrons move with $v_x \approx 0.5$, leading to the peak at $\gamma = \gamma(t = 0)$. Thus, the difference of curves A and B comes from the assumption of a uniform electron distribution over the angle φ'. This assumption becomes more reliable at later times ($t = 49.5$) and the difference between the two methods of spectrum computation vanishes (see curves C and D).

Therefore, the results of Vay's pusher coupled with the Landau-Lifshitz radiation reaction force or with the Monte Carlo event generator (which uses some approximate expression for fast computation of the emission probability) coincide well with the results obtained by other methods.

APPENDIX B: APPENDIX B: MULTIPOLE WAVE

In cylindrical coordinates the vector potential $\mathbf{A}$ of the current loop obeys the equation

$$\Delta A_\varphi - \partial_t^2 A_\varphi = -j_\varphi, \tag{B1}$$

where we assume that the z axis is the axis of the loop and thus $A_r = A_z = 0$. The solution of this equation for the harmonic current $j_\varphi \propto \exp(-i\omega t)$ (obviously, in normalized units $\omega = 1$) can be found using the Green's function as [53]

$$A_\varphi = -\frac{I_0 r_\ell}{\pi \bar{z}} \int_0^{\pi/2} \frac{\cos(2\psi)}{s} \exp(-it + is\bar{z}) d\psi, \tag{B2}$$

where I_0 is the current amplitude, $\bar{z} = [z^2 + (r + r_\ell)^2]^{1/2}$, $s = (1 - \kappa \sin^2\psi)^{1/2}$, and $\kappa = 4 r r_\ell / \bar{z}^2$. Then the electric and magnetic fields can be found from Eq. (B2).

To obtain the field of a multipole wave that is fully absorbed by the current loop, the substitutions $t \to -t$ and $B \to -B$ are made. Then the fields are computed on the r-z lattice and their values are used for the interpolation in the numerical solution of the equations of the electron motion.

[1] S. V. Bulanov, T. Z. Esirkepov, J. Koga, and T. Tajima, Plasma Phys. Rep. **30**, 196 (2004).

[2] A. Di Piazza, K. Z. Hatsagortsyan, and C. H. Keitel, Phys. Rev. Lett. **102**, 254802 (2009).

[3] R. Duclous, J. G. Kirk, and A. R. Bell, Plasma Phys. Controlled Fusion **53**, 015009 (2011).

[4] E. N. Nerush and I. Y. Kostyukov, Nucl. Instrum. Methods Phys. Res. A **653**, 7 (2011).

[5] A. G. R. Thomas, C. P. Ridgers, S. S. Bulanov, B. J. Griffin, and S. P. D. Mangles, Phys. Rev. X **2**, 041004 (2012).

[6] N. Neitz and A. Di Piazza, Phys. Rev. Lett. **111**, 054802 (2013).

[7] M. Vranic, T. Grismayer, R. A. Fonseca, and L. O. Silva, New J. Phys. **18**, 073035 (2016).

[8] J. M. Cole, K. T. Behm, E. Gerstmayr, T. G. Blackburn, J. C. Wood, C. D. Baird, M. J. Duff, C. Harvey, A. Ilderton, A. S. Joglekar, K. Krushelnick, S. Kuschel, M. Marklund, P. McKenna, C. D. Murphy, K. Poder, C. P. Ridgers, G. M. Samarin, G. Sarri, D. R. Symes, A. G. R. Thomas, J. Warwick, M. Zepf, Z. Najmudin, and S. P. D. Mangles, Phys. Rev. X **8**, 011020 (2018).

[9] K. Poder, M. Tamburini, G. Sarri, A. Di Piazza, S. Kuschel, C. D. Baird, K. Behm, S. Bohlen, J. M. Cole, D. J. Corvan, M. Duff, E. Gerstmayr, C. H. Keitel, K. Krushelnick, S. P. D. Mangles, P. McKenna, C. D. Murphy, Z. Najmudin, C. P. Ridgers, G. M. Samarin, D. R. Symes, A. G. R. Thomas, J. Warwick, and M. Zepf, Phys. Rev. X **8**, 031004 (2018).

[10] S. Corde, K. Ta Phuoc, G. Lambert, R. Fitour, V. Malka, A. Rousse, A. Beck, and E. Lefebvre, Rev. Mod. Phys. **85**, 1 (2013).

[11] G. Sarri, D. J. Corvan, W. Schumaker, J. M. Cole, A. Di Piazza, H. Ahmed, C. Harvey, C. H. Keitel, K. Krushelnick, S. P. D. Mangles, Z. Najmudin, D. Symes, A. G. R. Thomas, M. Yeung, Z. Zhao, and M. Zepf, Phys. Rev. Lett. **113**, 224801 (2014).

[12] W. Yan, C. Fruhling, G. Golovin, D. Haden, J. Luo, P. Zhang, B. Zhao, J. Zhang, C. Liu, M. Chen, and S. Chen, Nat. Photon. **11**, 514 (2017).

[13] C. P. Ridgers, C. S. Brady, R. Duclous, J. G. Kirk, K. Bennett, T. D. Arber, A. P. L. Robinson, and A. R. Bell, Phys. Rev. Lett. **108**, 165006 (2012).

[14] A. V. Bashinov and A. V. Kim, Phys. Plasmas **20**, 113111 (2013).

[15] E. N. Nerush, I. Y. Kostyukov, L. Ji, and A. Pukhov, Phys. Plasmas **21**, 013109 (2014).

[16] L. L. Ji, A. Pukhov, E. N. Nerush, I. Y. Kostyukov, B. F. Shen, and K. U. Akli, Phys. Plasmas **21**, 023109 (2014).

[17] H.-Z. Li, T.-P. Yu, J.-J. Liu, Y. Yin, X.-L. Zhu, R. Capdessus, F. Pegoraro, Z.-M. Sheng, P. McKenna, and F.-Q. Shao, Sci. Rep. **7**, 17312 (2017).

[18] E. N. Nerush, I. Y. Kostyukov, A. M. Fedotov, N. B. Narozhny, N. V. Elkina, and H. Ruhl, Phys. Rev. Lett. **106**, 035001 (2011).

[19] A. Gonoskov, A. Bashinov, S. Bastrakov, E. Efimenko, A. Ilderton, A. Kim, M. Marklund, I. Meyerov, A. Muraviev, and A. Sergeev, Phys. Rev. X **7**, 041003 (2017).

[20] M. Tamburini, F. Pegoraro, A. D. Piazza, C. H. Keitel, and A. Macchi, New J. Phys. **12**, 123005 (2010).

[21] M. Tamburini, T. V. Liseykina, F. Pegoraro, and A. Macchi, Phys. Rev. E **85**, 016407 (2012).

[22] R. Capdessus, E. d'Humières, and V. T. Tikhonchuk, Phys. Rev. E **86**, 036401 (2012).

[23] R. Capdessus and P. McKenna, Phys. Rev. E **91**, 053105 (2015).

[24] E. N. Nerush and I. Y. Kostyukov, Plasma Phys. Controlled Fusion **57**, 035007 (2015).

[25] E. G. Gelfer, A. M. Fedotov, and S. Weber, Plasma Phys. Controlled Fusion **60**, 064005 (2018).

[26] E. Gelfer, N. Elkina, and A. Fedotov, Sci. Rep. **8**, 6478 (2018).

[27] T. Grismayer, M. Vranic, J. L. Martins, R. A. Fonseca, and L. O. Silva, Phys. Plasmas **23**, 056706 (2016).

[28] P. Zhang, C. P. Ridgers, and A. G. R. Thomas, New J. Phys. **17**, 043051 (2015).

[29] T. V. Liseykina, S. V. Popruzhenko, and A. Macchi, New J. Phys. **18**, 072001 (2016).

[30] Y. B. Zel'dovich, Sov. Phys. Usp. **18**, 79 (1975).

[31] A. D. Piazza, Lett. Math. Phys. **83**, 305 (2008).

[32] I. Y. Kostyukov and E. N. Nerush, Phys. Plasmas **23**, 093119 (2016).

[33] M. A. Miller, Izv. Vyssh. Uchebn. Zaved. Radiofiz. **1**, 110 (1958).

[34] A. M. Fedotov, N. V. Elkina, E. G. Gelfer, N. B. Narozhny, and H. Ruhl, Phys. Rev. A **90**, 053847 (2014).

[35] A. Gonoskov and M. Marklund, Phys. Plasmas **25**, 093109 (2018).

[36] A. Gonoskov, A. Bashinov, I. Gonoskov, C. Harvey, A. Ilderton, A. Kim, M. Marklund, G. Mourou, and A. Sergeev, Phys. Rev. Lett. **113**, 014801 (2014).

[37] L. D. Landau and E. M. Lifshitz, *The Classical Theory of Fields* (Elsevier, Oxford, 1975).

[38] B. Le Garrec, S. Sebban, D. Margarone, M. Precek, S. Weber, O. Klimo, G. Korn, and B. Rus, in *High Energy/Average Power Lasers and Intense Beam Applications VII*, edited by S. J. Davis, M. C. Heaven, and J. T. Schriempf, SPIE Proc. Vol. 8962 (SPIE, Bellingham, 2014).

[39] http://www.eli-np.ro/.

[40] https://portail.polytechnique.edu/luli/en/cilex-apollon/apollon.

[41] https://www.clf.stfc.ac.uk/Pages/Vulcan-2020.aspx.

[42] A. V. Bashinov, A. A. Gonoskov, A. V. Kim, G. Mourou, and A. M. Sergeev, Eur. Phys. J. Spec. Top. **223**, 1105 (2014).

[43] V. B. Berestetskii, E. M. Lifshitz, and L. P. Pitaevskii, *Quantum Electrodynamics* (Pergamon Press, New York, 1982).

[44] N. V. Elkina, A. M. Fedotov, I. Y. Kostyukov, M. V. Legkov, N. B. Narozhny, E. N. Nerush, and H. Ruhl, Phys. Rev. Spec. Top.: AB **14**, 054401 (2011).

[45] V. N. Baier, V. Katkov, and V. Strakhovenko, *Electromagnetic Processes at High Energies in Oriented Single Crystals* (World Scientific, Singapore, 1998).

[46] J.-L. Vay, Phys. Plasmas **15**, 056701 (2008).

[47] http://iapras.ru/english/structure/dep_330/quill.html.

[48] E. N. Nerush, D. A. Serebryakov, and I. Y. Kostyukov, Astrophys. J. **851**, 129 (2017).

[49] A. V. Bashinov, P. Kumar, and A. V. Kim, Phys. Rev. A **95**, 042127 (2017).

[50] L. L. Ji, A. Pukhov, I. Y. Kostyukov, B. F. Shen, and K. Akli, Phys. Rev. Lett. **112**, 145003 (2014).

[51] A. Samsonov, E. Nerush, and I. Kostyukov, arXiv:1809.06115.

[52] A. Gonoskov, S. Bastrakov, E. Efimenko, A. Ilderton, M. Marklund, I. Meyerov, A. Muraviev, A. Sergeev, I. Surmin, and E. Wallin, Phys. Rev. E **92**, 023305 (2015).

[53] J. D. Jackson, *Classical Electrodynamics*, 3rd ed. (Wiley, New York, 1999).